Tribological and electrochemical performances of Cr/CrN and Cr/CrN/CrAlN multilayer coatings deposited by RF magnetron sputtering

N.E. Beliardouh [a,*], K. Bouzid [a], C. Nouveau [b], B. Tlili [c], M.J. Walock [d]

[a] Laboratoire d'Ingénierie des Surfaces (LIS), Université Badji Mokhtar, BP12 23000 Annaba, Algérie
[b] Laboratoire Bourguignon des Matériaux et Procédés (LaBoMaP), Arts et Métiers ParisTech de Cluny, Rue Porte de Paris, F-71250, Cluny, France
[c] Laboratoire Génie de Production (LGP), Ecole Nationale d'Ingénieurs de Tarbes, 47, avenue d'Azereix, BP1629, F-65016 Tarbes, France
[d] University of Alabama at Birmingham, Department of Physics, CH 310, 1720 2nd Ave S, Birmingham, AL35294-1170, USA

ARTICLE INFO

Article history:
Received 17 October 2013
Received in revised form
17 March 2014
Accepted 24 March 2014
Available online 18 April 2014

Keywords:
Multilayer
Cr/CrN/CrAlN
Wear
Corrosion

ABSTRACT

CrN/CrAlN and Cr/CrN/CrAlN multilayers were grown with dual RF magnetron sputtering. The application of these multilayers will be wood machining of green wood. That is why ball-on-disc and electrochemical tests in NaCl aqueous solution were realized to elucidate the tribological and corrosion behavior of these coatings as they will be exposed to wear and corrosion during wood machining process. The samples/alumina and samples/WC coupling showed different wear mechanisms. The 300 nm thick Cr/CrN/CrAlN multilayer demonstrated the best tribological behavior and corrosion resistance. The influence of growth defects on corrosion resistance has been shown.

1. Introduction

The physical vapor deposition (PVD) technique is well established as an environmentally friendly method to protect materials surfaces. Thus a variety of binary carbides and nitrides have been developed in the last three decades. Ternary compounds were obtained by adding a third element (transition metal) to traditional binary nitride films (CrN, TiN, AlN etc.) in order to increase mechanical and tribological properties. Further improvement in high-temperature properties of multicomponent (quaternary and higher systems) coatings can be achieved by the proper choice of additional alloying elements, such as Al, Si, Ti or Cr. Accordingly, for our part, we are interested in the addition of Al into the CrN system. This results in the formation of a metastable CrAlN ternary solution. Under operating conditions, this leads to the formation of complex aluminum and chromium oxides, which exhibit improved mechanical and tribological properties.

It is well known that Al and Cr additions can have a positive effect on the thermal stability and oxidation resistance of CrN and TiN based coatings, respectively [1–3]. The CrAlN films are probably the most promising coatings for high-temperature applications. Compared with TiAlN and AlTiN coatings, CrAlN presents better anti-spalling and anti-adhesion properties [4]. And, a high hardness (~30 GPa) and a high oxidation resistance temperature (900 °C) were reported for CrAlN coatings [5]. The effect of Al concentration in the Cr–Al–N system on its mechanical properties (hardness, elastic modulus, adhesion, oxidation…) as well as different wear behaviors has already been reported [6–8]. Sanchéz et al. [9] showed that high hardness (30 GPa), reduced elastic modulus (303 GPa), medium friction coefficient (0.45), high critical load (59 N), and good electrochemical behavior of Cr_{1-x} Al_xN coatings can be achieved at $x=0.54$. Wang et al. [10] reported that the simultaneous improvement of hardness and toughness is achievable when the negative bias voltage applied to the substrate is properly controlled. On the other hand, the incorporation of Al into the cubic CrN lattice can lead to increased roughness and porosity, as reported by Lee et al. [11]. As a consequence, the corrosion resistance of the CrAlN coating may be diminished, as shown by Sanchéz et al. [9]. To our knowledge, the exact Al concentration that must be incorporated into the Cr–N system to obtain optimal values of hardness and elastic modulus, simultaneously with high oxidation resistance has never been indicated in the literature [12,13].

To overcome some of these shortfalls, the surface engineering community has looked to the development of multilayered coatings. In terms of tribology, adhesion, and electrochemical properties, these coatings show better performance than their single-layer counterparts. CrAlN-based multilayered films with reasonable

* Corresponding author. Tel.: +213 (0) 338 891 2 83.
E-mail addresses: beliardouh_23@yahoo.fr (N.E. Beliardouh), kheiro.bouzid@yahoo.fr (K. Bouzid), corinne.nouveau@ENSAM.EU (C. Nouveau), tlilii_brahim@yahoo.fr (B. Tlili), mwalock@uab.edu (M.J. Walock).

properties, such as CrAlN/AlON [14],CrN/CrAlN [15], CrAlN/BN [16] and TiAlN/CrAlN [17], have been developed. In addition to improving the tribological, adhesive, and electrochemical properties of the coatings, the mechanical properties can also be improved. For example, the hardness can be increased with a decrease in the CrAlN layer thickness. A maximum hardness of 34.7 GPa was obtained for a 3 nm thick CrAlN layer in a study on CrAlN/AlON multilayer coatings [14]. Nanoindentation tests reveal a hardness ranging from 37 to 46 GPa in case of CrN/CrAlN multilayer thin films [15].

Another opportunity for improvement is the mechanical response at high temperatures. CrAlN/BN coatings show superior oxidation resistance compared to CrAlN coatings. After annealing at 800 °C in air for 1 h, the hardness of CrAlN coatings decreased to 50% of the as-deposited ones; in contrast, the hardness of CrAlN/BN nanocomposite coatings stayed the same, or in some cases increased to about 46 GPa, as revealed by Nose et al. [16]. Recently, Li et al. [18] developed a ZrO_2/CrAlN multilayer and obtained excellent mechanical properties at elevated temperatures. After annealing at 1000 °C for 30 min, the hardness and elastic modulus were as high as 36.8 and 465.7 GPa, respectively. Another study [17] reported that TiAlN/CrAlN multilayer coatings have high hardness (~38 GPa) and adhesive strength (~98 N) with the thermal stability of TiAlN and the oxidation resistance of CrAlN.

Yet, for all this research into multilayer coatings, only a few studies report simultaneously on the wear and electrochemical behavior of multilayer coatings based on Cr–X–N (X=transition metal). In previous work [19], the physical and mechanical properties of multilayer CrAlN-based coatings were reported. In this work, we conduct a comparative study of the wear and electrochemical behavior with respect to the hardness, total coating thickness, and the role of a Cr underlayer. Indeed, overriding goal of our research is the development of a new protective multilayer coating system to improve the service life of cutting tools in wood machining. They would be submitted to wear (abrasion, shocks etc) but also to corrosion (machining of green/wet wood) that is why our study focused on the tribological (pin-on-disc tests) and corrosion behavior (using potentiodynamic polarization and electrochemical impedance spectroscopy measurements) of the coatings.

2. Experimental details

2.1. Materials

Multilayer coatings of CrN/CrAlN and Cr/CrN/CrAlN (Fig. 1) were deposited on mechanically polished steel substrates (AISI 4140; H=4.1 GPa) at 200 °C, using a radio frequency (RF) dual magnetron sputtering system (NORDIKO type 3500), operating at 13.56 MHz and equipped with two confocal sputtering guns. The Cr and Al targets had purity levels of 99.95% and 99.999%, respectively. The distance from target to substrate was fixed at 100 mm and the applied bias voltage was −300 V and −900 V for Al and Cr respectively. The deposition conditions of the studied multilayers are described in detail elsewhere [19,20]. Besides, the physico-chemical (composition, thickness), structural (XRD patterns), mechanical (stress, hardness, Young's Modulus) and thermal properties of these multilayers systems were also determined in these previous works [19,20]. The chemical compositions (Scanning Electron Microscopy (Jeol JSM 5900 LV) equipped with Energy Dispersive Spectroscopy (EDS))and some characteristics of coatings are given in Table 1. The average value of surface roughness, estimated by optical profilometry(VEECO, Wylo NT-1100), was 0.056 ± 0.004 μm.

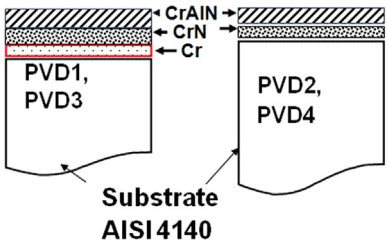

Fig. 1. Scheme of the multilayer systems on steel substrate.

2.2. Tribological tests

Dry wear tests were carried out using a ball-on-disc tribometer (CSM Instruments), which continuously records the coefficient of friction (COF) as a function of time/sliding distance. The tribological tests parameters are summarized in Table 2. The counterparts were alumina (H=16.14 GPa) and WC- 6%Co ball (H=15 GPa), 6 mm in diameter (supplied by CSM Instruments). Alumina and WC are widely used as standard counterparts for tribological tests. These materials have a higher hardness than steel and as we expect abrasion and shocks during wood machining process they are more suitable to test the wear resistance of our coatings. Besides, we could compare the COF of our coatings in contact with materials that have different roughness (Table 2) (many wood species of different surface state are machined and then the range of wood/coating COF is large).

A proprietary software package was used to control the experimental set-up and provide data handling. The velocity and applied load have been chosen according to the tribometer limits and to previous studies [20] (Table 2). The wear track diameter depends on the balls diameter, the velocity and the applied load. A sliding distance of 200 m permits to observe the wear of the entire coatings (until their disappearance from the substrate). Tests were conducted at room temperature (20 °C) with a relative humidity below 40% to almost reproduce wood manufacture conditions (in air or moderate room temperature, wet wood machining).

An optical profilometer (VEECO-Wyko NT1100) was used to measure the cross-section of the wear track at several locations. Based on

Table 1
Coatings properties obtained by RF dual magnetron sputtering.

PVDi	Multilayer thickness (nm)	Hardness (GPa)	Adhesion L_{C1} (N)	Chemical composition (at%)		
				N	Al	Cr
PVD1	(Cr/CrN/CrAlN) (~132/~368/~1000)	26	78	51.8	4.2	42.9
PVD2	CrN/CrAlN (~150/~150)	22	40	50.8	4	43.1
PVD3	Cr/CrN/CrAlN (~45/~106/~150)	32	56	50.5	4.7	42.5
PVD4	CrN/CrAlN (~500/~1000)	17	40	52	5	41.3

Table 2
Tribological tests parameters.

Applied load (N)		1
Velocity (m/s)		0.01
Total sliding distance (m)		200
Wear track diameter (mm)		4
Ball diameter (mm)		6
Roughness of balls (R_a, μm)	Alumina	1.52
	WC	0.388
Environment		Air
Temperature (°C)		20 ± 3
Humidity (%)		40 ± 5

classical equations, the volume loss of the coated samples was calculated. Three wear tests were performed per sample. The quantification of the ball's wear volume loss was not easy, however, a semi-quantitative calculation is possible for comparison. Thus volumetric wear of the static counterparts (balls) was estimated using the volume loss calculation from the spherical crown of the ball measured by optical microscopy and optical profilometry.

2.3. Electrochemical tests

Electrochemical tests were conducted in a 3.0 wt% NaCl aqueous solution, with distilled water, under free air condition at room temperature (22 °C). The study was carried out with a GAMRY Model PCI 4 unit used for DC and AC measurements. Electrochemical Impedance Spectroscopy (EIS) and Tafel polarization curve techniques were measured in a cell (volume of 200 ml) with the multilayer coating as the working electrode, an Ag/AgCl reference electrode and a platinum wire as the counter-electrode. EIS measurements were initiated at the stable Open Circuit Potential values, which were determined after 24 h of exposure. For our Nyquist diagrams, frequency sweeps were conducted in the range 100 kHz to 0.01 Hz, using sinusoidal voltage perturbation with signal amplitude of 30 mV. The Tafel polarization curves were obtained at a sweep speed of 0.5 mV/s in voltage ranging from −0.4 to +0.4 V.

3. Results and discussion

3.1. Coefficient of friction variation

Fig. 1 shows the evolution of the COF as a function of sliding cycles for the multilayer coatings, against the (a) alumina and (b) WC counterparts. Against both counterparts, each multilayer sample shows typical running-in behavior: an initial transient state followed by an increase in the COF until it reaches a steady state. The initial transient state corresponds to contact between the highest asperities of the disk and the static partner's surface. Vibrations and noise are also present in the data.

3.1.1. Alumina ball

Against alumina, the COF of (Cr/CrN/CrAlN)-PVD1 is 0.38 at the beginning of the test, shows a short run-in period, which is followed by an increase to 0.6. From here, the wear becomes more severe, which leads to coating failure and a higher COF value (~1.05). The (Cr/CrN/CrAlN)-PVD3 coating presents a short run-in followed by a long period of constant COF (~0.4), corresponding to steady state.

The COF of (CrN/CrAlN)-PVD2 begins at 0.3, increases slowly to around 0.55–0.6. A sudden change in friction behavior corresponds to breakthrough of the (CrN/CrAlN)-PVD2 coating after 2500 cycles, as shown in Fig. 2(a). With the (CrN/CrAlN)-PVD4 coating, the COF showed dissimilar behavior: the COF is very low at the beginning (0.2) but quickly reaches higher values. This is probably due to high wear and coating's delamination.

Against alumina balls, only the (Cr/CrN/CrAlN)-PVD3 coating survives the tribological tests. As shown in Table 1, the (Cr/CrN/CrAlN)-PVD3 coating has the highest hardness. It presents the best wear behavior (against the alumina counterpart) in comparison to the (Cr/CrN/CrAlN)-PVD1, (CrN/CrAlN)-PVD2 and (CrN/CrAlN)-PVD4 coatings. Thus, we can conclude that the (Cr/CrN/CrAlN)-PVD3 coating improves the friction behavior against Al_2O_3 balls in comparison to other multilayer systems.

3.1.2. WC balls

Fig. 2(b) shows the plots for (Cr/CrN/CrAlN) and (CrN/CrAlN) coatings against WC balls. For all tribological couples, the evolution

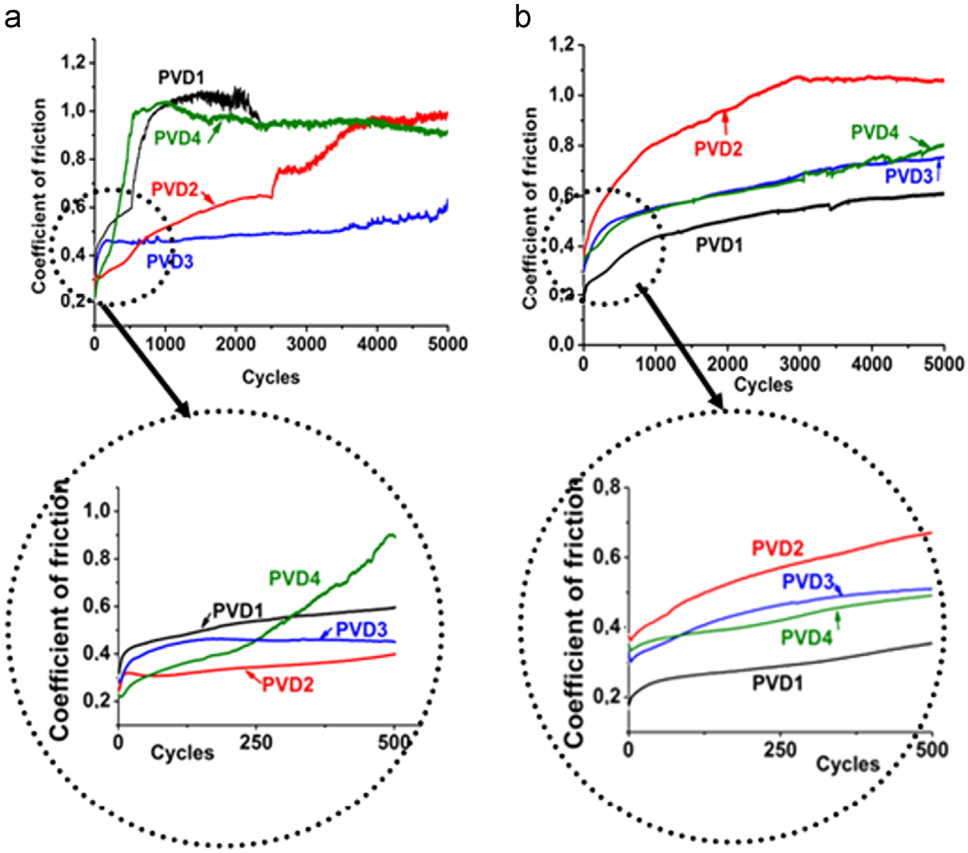

Fig. 2. Coefficient of friction variation of each antagonist couple against (a) alumina and (b) WC–Co ball.

of the COF shows the same tendency at the beginning of the test: a run-in process followed by the gradually increase to a steady state condition. However, the slopes of these curves slowly increase, without the abrupt rises observed against the alumina counterparts. The (Cr/CrN/CrAlN)-PVD1 coating shows the lowest COF value, while the (CrN/CrAlN)-PVD2 has the highest COF. Therefore, we have improved the friction behavior of the AISI 4140 steel, against WC balls, with the adoption of the (Cr/CrN/CrAlN)-PVD1 coating system. The (Cr/CrN/CrAlN)-PVD3 and (CrN/CrAlN)-PVD4 coatings show practically similar COF evolutions; their curves overlap throughout a sliding distance of 200 m. This occurs despite the differences in overall thickness and hardness between the two coating systems.

3.2. Wear analysis

Dry sliding leads to high local pressure between contacting asperities, which results in plastic deformation, adhesion, and the consequent formation of local junctions. Wear debris are composed of the particles spalling from the pin, a stationary part considered as an upper part, and from the disc, a dynamically active part having specific sliding velocity considered as a lower specimen during the wear process.

3.2.1. Wear track of coatings

3.2.1.1. Alumina balls. Fig. 3(a) and (b) show an example of the wear track observed by SEM on (Cr/CrN/CrAlN)-PVD3. Wear debris accumulated were observed in the first region (for example: area 1 in Fig. 3 (a)), localized at the side of the wear track. EDS analyses reveal the presence of Fe (substrate), Cr and Al (elements from the coating and possibly the counterpart) and oxygen. These elements were also detected in the second region (area 2, Fig. 3(b)), which is the light region localized in the middle of the wear track. These areas were oxidized due to the localized high temperature caused by friction during dry sliding; the surface (top layer) reacts with oxygen in the ambient atmosphere forming oxides. We did not detect any nitrogen in the different regions of the wear scar. Relatively smooth regions can be also observed (area 3 in Fig. 3(b)). In this area, only elements of the substrate were detected indicating local delamination of the coating. Small particles of wear debris were also observed. They were probably removed from the material via plastic deformation. In addition, grooves parallel to sliding direction, are clearly visible (indicated by arrows in Fig. 3(b)). To conclude, against alumina balls, the wear mechanism of (Cr/CrN/CrAlN) multilayer coatings (PVD1 and PVD3) was an oxidative wear with some mild abrasive and adhesive wear.

An example of wear tracks of (CrN/CrAlN) multilayer coatings is shown in Fig. 3(c). EDS analyses indicate that the regions of the edges of wear track (area 1′ in Fig. 3(c)) are constituted by elements of the coating, elements of the substrate and oxygen. No coating elements and no oxygen could be found in the central regions of the wear track (area 2′ in Fig. 3(c)); the coating was completely delaminated. An example of the 3D profile, as evaluated by optical profilometry, is illustrated in Fig. 3(d) and confirms the complete delamination of the coating in the central region of track. SEM images (Fig. 3(c)) show plowed grooves along the sliding direction and debris piled up on the edges of the wear track. The debris were identified by EDS as a mixture of Cr, Al, Fe, O, (area 3′ in Fig. 3(c)). Therefore, observations suggest the following: at the beginning of sliding, the wear mechanism was oxidative; as sliding progresses, it changed to abrasive and adhesive wear.

The difference in the COF variation between (Cr/CrN/CrAlN) and (CrN/CrAlN) coatings (Fig. 2(a)) can be related to the differences in the hardness between coatings and oxides (third body). Tribo-oxidation plays an important role in controlling friction between ball and disc surface and affects the wear behavior of the coatings, as reported in literature [12,21]. Besides, the friction force depends on asperity deformation, ploughing of wear particles and surface adhesion [22].Thus, the oxides produced during sliding process reduce friction, acting as lubricant in the case of

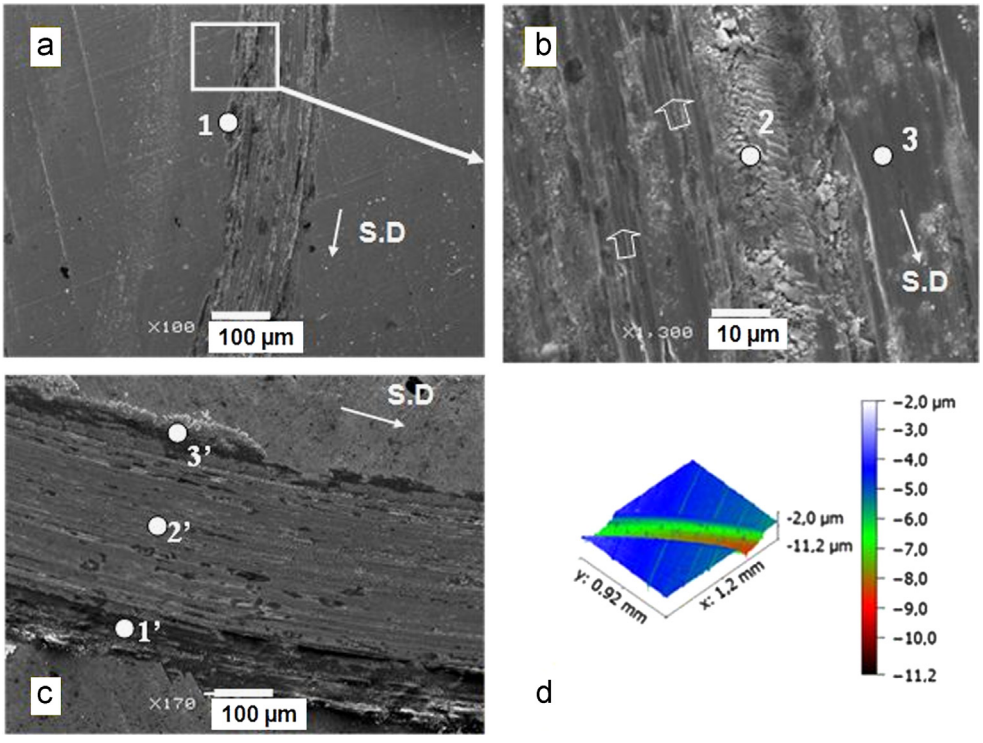

Fig. 3. SEM images of (a) and (b) (Cr/CrN/CrAlN)-PVD3, (c) (CrN/CrAlN)-PVD4, against alumina balls and (d) example of 3D wear track topography as a function of depth (corresponding to (c)).

(Cr/CrN/CrAlN)-PVD3 while they play an abrasive role in other cases.

3.2.1.2. WC balls. Fig. 4(a) and (b) show the SEM images of worn surfaces of the (Cr/CrN/CrAlN)-PVD1 and (CrN/CrAlN)-PVD4, respectively. Here, the first phenomenon observed was the concentrated wear in the middle of the wear track. EDS analyses reveal different regions and quantities of wear debris accumulated at the edges of the wear tracks of (Cr/CrN/CrAlN)-PVD1 (Fig. 4(a)). The dark regions (area 1 in Fig. 4(a)) are constituted by elements of the coating, elements of the counterpart and oxygen. However, in the middle of tracks (area 2 in Fig. 4(a)), elements of the coating, substrate, counterpart and oxygen are detected. The light regions (area 3 in Fig. 4(a)) were composed exclusively of coating elements indicating that the coating has yet to completely delaminate.

The (CrN/CrAlN)-PVD4 coating exhibits a larger wear track and extensive cracking in the middle region can be seen in Fig. 4(b). The debris compaction in area 1′ was investigated by EDS analyses (Fig. 4 (c)), which reveal elements of the coatings, counterpart, oxygen and substrate. In area 2′ (Fig. 4(b)), the substrate as well as counterpart elements and oxygen were detected. Oxygen and transferred element from the counter body (W, Co) were also detected in the area 3′ in Fig. 4(b). Inside the wear track, there is no area free of oxides as with the above-mentioned coatings (area 3 in Fig. 4(a)). It was obvious that (CrN/CrAlN)-PVD4 was strongly worn in comparison to (Cr/CrN/CrAlN)-PVD1. Thus, when WC balls are the counter face, an oxide layer formed at the interface between the counter body and the coatings' surface. A mixture of the coating, various oxides and transferred material from WC ball turned into a debris layer by the continually rubbing, grinding and compacting occurring during the tribotest. As sliding progresses, additional tungsten and oxygen were incorporated into the CrAlN top layers. The latest became more brittle, and consequently exhibited cracks. Cracked coatings will be easily delaminated into large pieces of debris, which builds up inside the wear track, by a means of adhesive failure. To conclude, adhesion seems to be the main wear mechanism with some oxidative wear during the tribological tests of the (Cr/CrN/CrAlN) and the (CrN/CrAlN) multilayer coatings against WC balls.

3.2.2. Wear scar of balls

The wear scars on the alumina and WC balls, obtained against the PVD1 multilayer, are shown in Fig. 5. Before tribological tests, the balls, sample-holder and coated samples were cleaned together in an ultrasonic bath with alcohol, then dried under pressured air; the initial states of balls' surfaces are shown in Fig. 5 (a) and (a′)). At the end of the tests, the ball wear scars were observed by optical microscopy (Fig. 5(b) and (b′)). Subsequently, each ball scar reveals details of the different wear mechanisms. Afterwards, the balls are cleaned in distilled water, immerged in an ultrasonic bath and dried under pressured air. Then, the wear scar dimensions can be easily determined to estimate the volume loss (Fig. 5(c) and (c′)). The alumina and WC balls used as counterparts in this study exhibit a similar form of "calotte" scar: ball scars are elliptical in the case of alumina while scars are circular for WC balls.

Following a tribotest, the wear scars of the alumina counterparts were covered by adhered material (wear product), as shown in the optical image (Fig. 5(b)). After cleaning, micro grooves were also revealed (Fig. 5(c)). Therefore, third-body wear occurred when the Cr/CrN/CrAlN coatings were sliding against the alumina balls; in addition, there is evidence of mild abrasive and adhesive wear. The same mechanism occurs with alumina ball/CrN/CrAlN couples.

Grooves and scratches along the sliding direction were also observed on the wear tracks of the WC balls (Fig. 5(c′)). This provides unambiguous evidence of hard particles scratching, or plowing the counter body; Cr_2O_3 is mentioned in the literature [23] as a prime candidate for this behavior. Abrasive wear is the main mechanism for WC counter body wear.

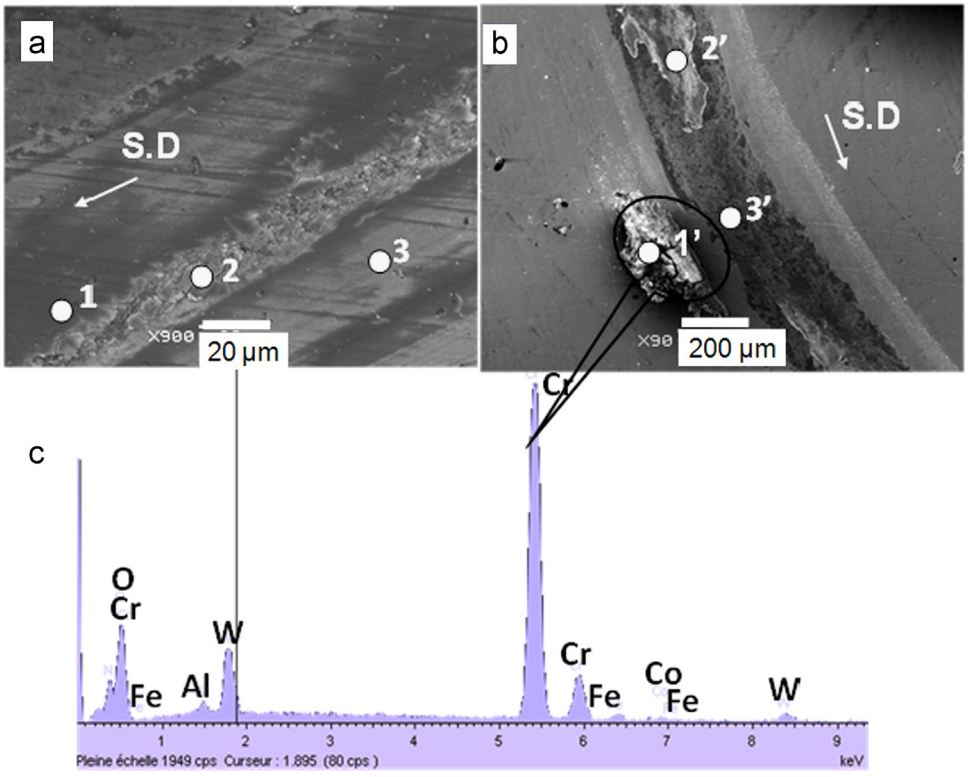

Fig. 4. SEM images of (a) (Cr/CrN/CrAlN)-PVD1and (b) (CrN/CrAlN)-PVD4 wear track against WC ball, (c) EDS spectra of point 1.

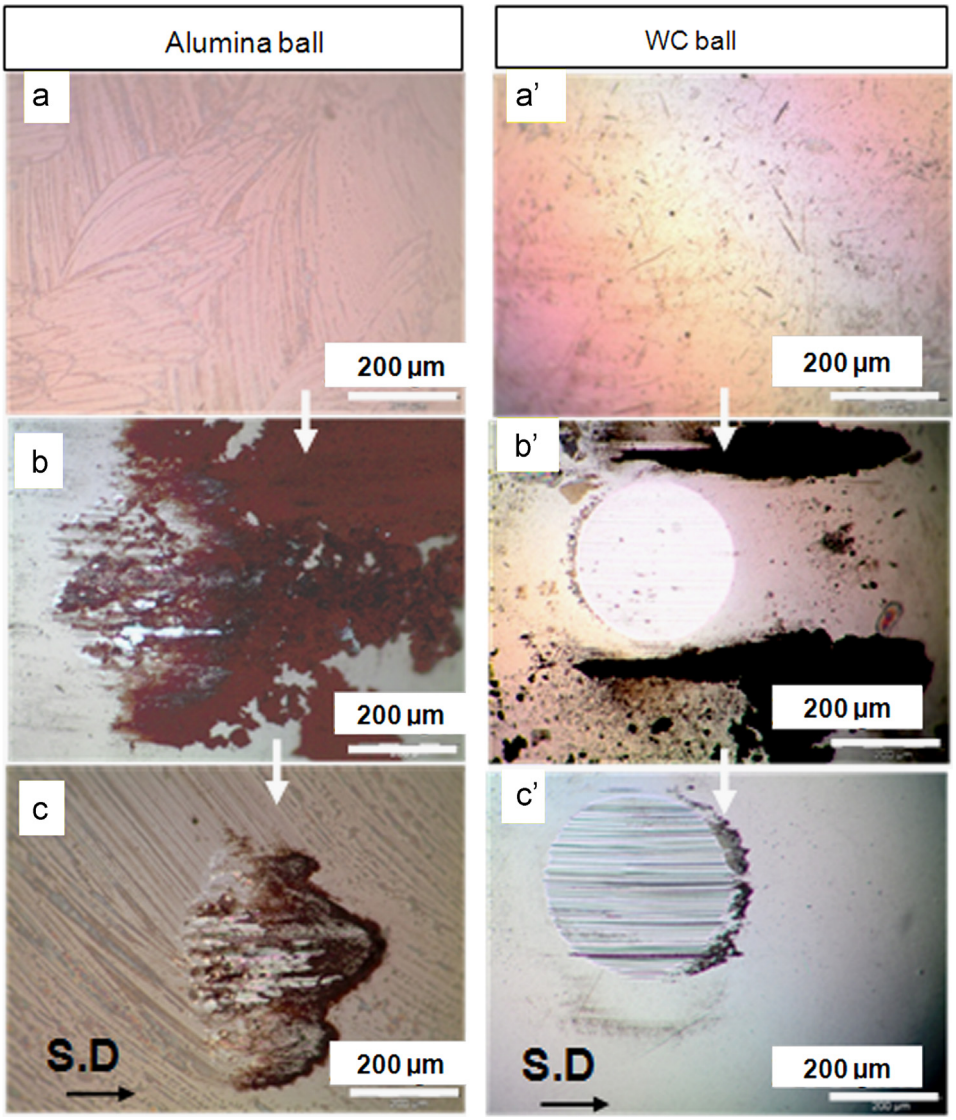

Fig. 5. Optical images of a typical wear scar on an alumina (a)–(c) and a WC (a′)–(c′) ball against (Cr/CrN/CrAlN)-PVD1 multilayer coatings after 200 m sliding distance: (a) and (a′) initial state, (b) and (b′) after the test and (c) and (c′) after cleaning.

3.2.3. Volumetric wear

The estimated wear volume for each couple (PVDi/ball) is presented in Fig. 6. The results can be summarized as follows:

- For the coatings, the alumina balls produced the highest amount of wear, with the extreme (i.e. worst) being the (CrN/CrAlN)-PVD4/alumina couple. The WC balls produced the lowest wear, with the extreme (i.e. best) being the (Cr/CrN/CrAlN)-PVD1/WC couple.
- For the counterparts, the coatings produced the least amount of wear damage on the alumina balls, and the highest wear damage on the WC balls. This may be related to the higher hardness of the alumina balls compared to the WC balls.
- It is interesting to note that the (CrN/CrAlN)-PVD4/alumina couple presented the highest sample/disc wear volume, and the (CrN/CrAlN)-PVD4/WC couple presented the highest counterpart wear volume.

From the above results and discussions it is obvious that the Cr underlayer enhances the wear behavior of the multilayer coatings. Furthermore, it has been observed that sliding wear property of specimen depends on the counter face materials. These results are in agreement with many studies among others [24–27]. Under our tribological tests parameters, the (Cr/CrN/CrAlN)-PVD3 presents the lowest COF and also the lowest wear volume loss against alumina balls, while better tribological behavior is shown by the (Cr/CrN/CrAlN)-PVD1coupling against WC balls. This result can be related to the wear mechanism between surfaces in contact and to the thickness ratio of CrN/CrAlN [27,28].

The morphology of debris formed during sliding of coatings against the counterpart material i.e. form that allows them to roll, reduced the friction. Besides, lubricating oxides such as Cr_2O_3 or Cr–Al–O, are well known to play important role in reduction of COF [29]: the more lubricating oxides we have, the best is the wear resistance. So, in agreement with the literature [30], high hardness of the thin film is not necessarily the main parameter to obtain a good wear resistance.

3.3. Electrochemical tests

Usually, a thin film of a transition metal nitride would provide excellent protection to a substrate against corrosion in several environments. They are inert to chemical attacks due to their relatively higher position in electrochemical series [31].Unfortunately, in an

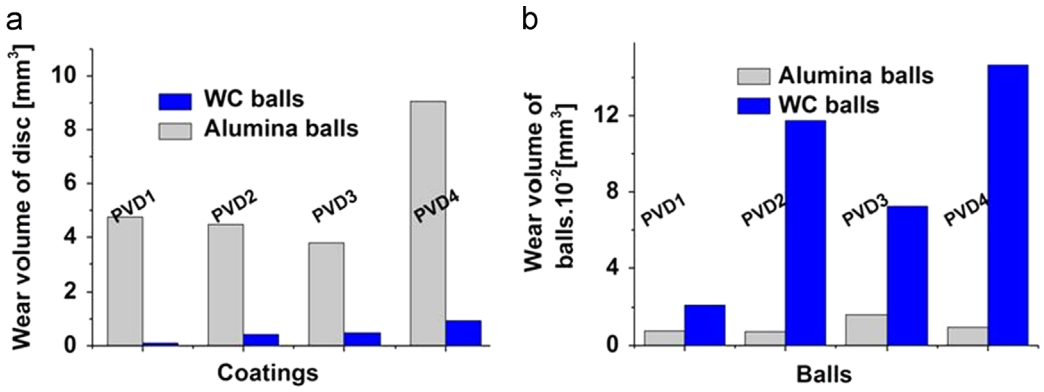

Fig. 6. Estimated wear volume of (a) multilayer coatings and (b) balls.

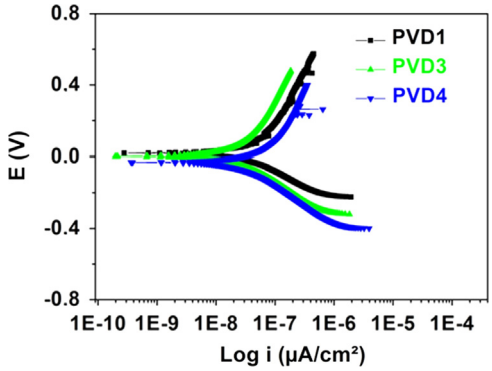

Fig. 7. Potentiodynamic polarization curves (Tafel curves) of the different multilayer coatings.

aggressive environment, these coatings are not as effective. This is probably due to porosity, pinholes, droplets and other growth defects formed during the PVD deposition process. When the coated sample is immersed in an aggressive environment, corrosion is expected to initiate at these defect sites on the coatings' surface. This leads to localized galvanic cell formation [32,33]. Cracks, pinholes, and pores allow the corrosive media to enter the substrate, which further degrades the corrosion behavior of the coating and/or substrate system. One method to alleviate this behavior is by depositing a multilayer coating rather than a single layer coating. The increased number of interfaces can significantly improve the corrosion resistance of the coating/substrate system [34,35].

Like wear, corrosion can occur via numerous mechanisms. The details of these different corrosion mechanisms are schematized and explained in the literature [31]. The main feature of these corrosion mechanisms is water reduction at the cathodic site and metal oxidation at the anodic site, following the reactions:

$$\text{Anode: } Me \rightarrow Me^{n+} + ne^{-} \quad (1)$$

$$\text{Cathode: } 2H_2O + 2e^{-} \rightarrow H^2 + 2OH^{-} \quad (2)$$

These two competing reactions may occur on the electrode surface, working from the outer surface towards the substrate [36]. In such cases, the electrochemical interface can generally be divided into two or three sub interfaces: electrolyte/coating, electrolyte/droplet and electrolyte/substrate [37]. Marulanda et al. [38] suggest that the improvement of multilayer corrosion resistance was probably due to interfacial blocking of the propagation of microcracks and dislocations, coupled with avoiding pinhole/pore continuity. In this study, we attempt to understand different corrosion mechanisms by the electrochemical performance of coated samples in contact with aggressive chloride ions (Cl^-).

Table 3
Corrosion results obtained from the Tafel curve measurements.

Coatings	E_{corr} (mV)	I_{corr} (nA)	$V_{corr} \times 10^{-3}$ (mm/y)
PVD1	18.2	92.1	68.35
PVD3	1.71	42.3	31.39
PVD4	−31.2	58.5	43.40

3.3.1. Potentiodynamic polarization tests

Fig. 7 shows the Tafel polarization curves for samples exposed to the 3.0 wt% NaCl solution for 24 h. From these curves, we can find the anodic and cathodic slopes. The corrosion potential (E_{corr}) and the corrosion current density (I_{corr}) for multilayer coatings are calculated from the polarization curves by fitting the Tafel equation. The results of the electrochemical measurements are summarized in Table 3.

As shown, all of the tested coatings exhibited passive behavior and good corrosion resistance. The (Cr/CrN/CrAlN)-PVD3 coating presents the best corrosion resistance with a positive potential (E_{corr}), and the lowest corrosion current densities (I_{corr}) [31,33,39]. This result has a direct relationship with the corrosion velocity, also shown in Table 3.

3.3.2. Electrochemical impedance spectroscopy measurements

The different Nyquist diagrams are presented in Fig. 8(a). It is obvious that the (Cr/CrN/CrAlN)-PVD3 coating presents the best corrosion resistance followed by (CrN/CrAlN)-PVD4. All of the Nyquist plots show two time constants, with a capacitive loop of smaller diameter followed by another capacitive loop of larger diameter. Bode plots, of the phase angle as a function of the frequency (semi logarithm scale) are shown in Fig. 8(b) and confirm the Nyquist data. From the above mentioned results, it is confirmed that there are effectively two time constants in the experimental frequency bandwidth. Consequently, the EIS data indicates the existence of two different interfacial reactions that may be related to the coating/solution interface and substrate/solution interface, respectively.

The experimental results were interpreted through the development of typical impedance models for the electrode surfaces, and curve fitting on the basis of an equivalent circuit (using the Zview impedance program). A circuit model was proposed to ascribe the two sub-electrochemical interfaces that are generally used in such cases [32,33,36,37]. The equivalent circuit (Fig. 8(c)) consists of the following elements: R_s corresponds to the solution resistance of the electrolyte test between the working electrode (WE) and reference electrode (RE). *CPE1* and R_{po} elements were used in parallel to replace the coatings' dielectric properties. *CPE2*

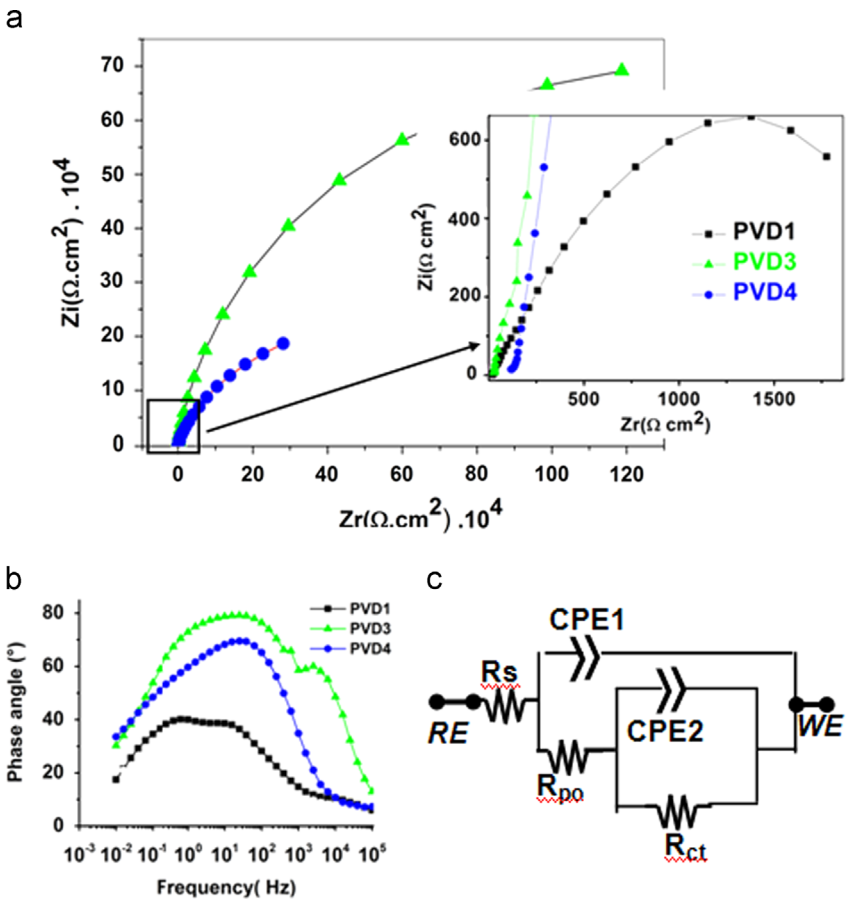

Fig. 8. AC impedance measurements of the multilayer coatings (a) Nyquist impedance diagrams (inset image shows the Nyquist plots at high frequencies), (b) bode plots and (c) the equivalent circuit model used to fit impedance EIS data.

and R_{ct}, in parallel, were adopted to describe the charge transfer at the coating/substrate interface.

Results of the fitting values obtained from the equivalent circuit simulation of the different coating configurations are summarized in Table 4. These results seem to indicate that the thickest coating system had a lower CPE1 value and higher charge transfer resistance. Chipatecua et al. [35] explained that electrolyte diffusion through the thinner coating took less time because of shorter path length, and rapidly produced a dense, passive oxide film at the bottom of the permeable defects.

The total polarization resistance (R_p) is taken as the sum of all resistances obtained from the EIS results [31,33,35,38,40]:

$$R_p = R_{po} + R_{ct} \quad (3)$$

R_p can be considered as an indicator of the corrosion resistance of the material, which is inversely proportional to the corrosion velocity [11,41]. This confirms our earlier results that the (Cr/CrN/CrAlN)-PVD3 coating presents the highest corrosion resistance and the best electrochemical behavior when immersed in the 3 wt% NaCl aggressive solution (Table 4). The R_p of (Cr/CrN/CrAlN)-PVD3 and (Cr/CrN/CrAlN)-PVD4 was around 3000 kΩ and 800 kΩ, respectively, indicating their high corrosion resistance. These results are also in good agreement with the potentiodynamic polarization measurements.

3.3.3. SEM investigations

Fig. 9 presents the surface morphology of the (CrN/CrAlN)-PVD4 coating after 24 h of immersion during potentiodynamic test in a 3 wt% NaCl solution. Significant macro particles, droplets and growth defects, which were probably formed during sputtering process, can be observed on the surface of the coating in addition to various pinholes and craters. SEM images can prove that selective corrosion occurs at growth defect sites. According to Lewis et al. [42], a droplet is compositionally metal rich and nitrogen deficient; this defect is anodic with respect to both surrounding coating. It is obvious on Fig. 9(b) that the corrosive attack occurs with the ejection of droplets from the coatings which creates a crater at its surface, resulting in direct contact with the substrate.

Finally, our study indicates that all of our CrN/CrAlN and Cr/CrN/CrAlN multilayer coatings present better behavior against aggressive chloride ions (Cl^-) when compared to similar CrAlN based coatings, as reported in other studies [35,37,38,41,42]. Yet, each of our coatings exhibited different electrochemical behaviors. This occurred despite the same chemical composition and phase microstructure of the outer CrAlN layer. We are in agreement with Lv et al. [13] and believe that the different electrochemical behavior of our multilayer may be associated with their different surface defect densities.

Table 4
Optimized values for the equivalent circuit parameters obtained by ZView program simulation.

Coatings	R_s (Ω)	CPE1 (F.s^(a-1))	a_1	R_{pore} (Ω)	CPE2 (F.s^(a-1))	a_2	R_{ct} (Ω)
PVD1	25	0.236E−3	0.7854	180.7	1.087E−3	0.6	2326
PVD3	31	2.358E−6	0.8301	1.232E6	7.904E−6	0.65	1.861E6
PVD4	28	9.279E−6	0.7061	0.321E6	16.39E−6	0.6	0.503E6

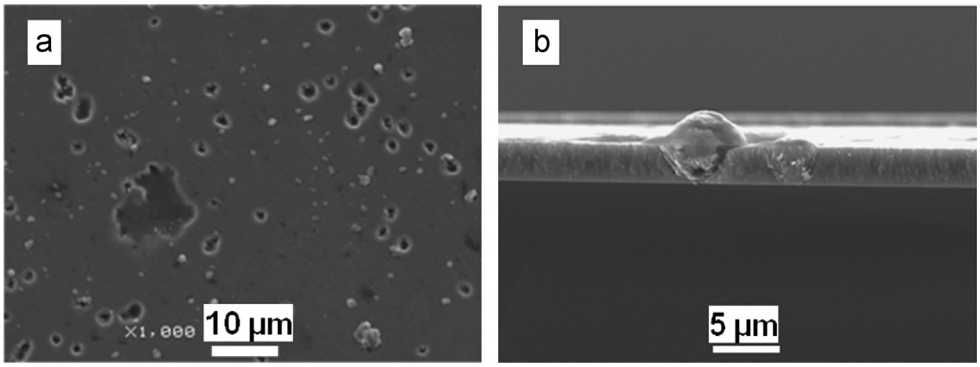

Fig. 9. SEM images of (a) (CrN/CrAlN)-PVD4 multilayer coatingsuperficial surface morphology after 24 h exposure to a 3.0% NaCl solutionand (b) a cross-section showing a crater after droplet ejection.

4. Conclusion

Accordingly, we conclude that:

- Alumina counterparts cause significantly more wear to our multilayer coatings than WC–Co counterparts.
- While the cause it is not known, it appears that there is some beneficial action from the Cr underlayer on the COF variation.
- SEM-EDS analysis of the post-tribotest samples reveal that:
  - Sample/alumina couples underwent abrasive and adhesive wear mechanisms after an oxidative wear behavior.
  - Sample/WC–Co couples underwent similar behavior: oxidative wear followed by abrasive wear.
- EIS was used to measure the polarization resistance of the deposited coatings. From these results, we conclude that the (Cr/CrN/CrAlN)-PVD3 coating system has the optimal electrochemical behavior. Growth defect density seems to have a more significant effect on the corrosion behavior than the coating's other properties, such as thickness, microstructure and mechanical properties.
- It should be noted that the (Cr/CrN/CrAlN)-PVD3 coating shows not only the best electrochemical behavior, but also the best tribological protection as well. Further investigations are necessary to determine if there is any relationship.

Acknowledgments

The authors would like to thank Mr. Romain FLITI, Mr. Denis LAGADRILLERE for experimental support and Pr. Sihem ABDER-RAHMANE for helpful discussions.

References

[1] Kiryukhantsev-Korneev PhV, Shtansky DV, Petrzhik MI, Levashov EA, Mavrin BN. Thermal stability and oxidation resistance of Ti–B–N, Ti–Cr–B–N, Ti–Si–B–N and Ti–Al–Si–B–N films. Surf Coat Technol 2007;20:6143–7.
[2] Kuptsov KA, Kiryukhantsev-Korneev PhV, Sheveyko AN, Shtansky DV. Comparative study of electrochemical and impact wear behavior of TiCN, TiSiCN, TiCrSiCN, and TiAlSiCN coatings. Surf Coat Technol 2013;216:273–81.
[3] Gannon PE, Tripp CT, Knospe AK, Ramana CV, Deibert M, Smith RJ, et al. High-temperature oxidation resistance and surface electrical conductivity of stainless steels with filtered arc Cr–Al–N multilayer and/or superlattice coatings. Surf Coat Technol 2004;189:55–61.
[4] Aihua L, Jianxin D, Haibing C, Yangyang C, Jun Z. Friction and wear properties of TiN, TiAlN, AlTiN and CrAlN PVD nitride coatings. Int J Refract Met Hard Mater 2012;31:82–8.
[5] Brizuela M, Garcia-Luis A, Braceras I, Oñate JI, Sánchez-López JC, Martínez-Martínez D, et al. Magnetron sputtering of CrAlN coatings: mechanical and tribological study. Surf Coat Technol 2005;200:192–7.
[6] Kim GS, Lee SY. Microstructure and mechanical properties of AlCrN films deposited by CFUBMS. Surf Coat Technol 2006;201:4361–6.
[7] Pulugurtha SR, Bhat DG, Gordon MH, Shultz J, Staia M, Joshi SV, et al. Mechanical and tribological properties of compositionally graded CrAlN films deposited by AC reactive magnetron sputtering. Surf Coat Technol 2007;202:1160–6.
[8] Chunyan Y, Linhai T, Yinghui W, Shebin W, Tianbao L, Bingshe X. The effect of substrate bias voltages on impact resistance of CrAlN coatings deposited by modified ion beam enhanced magnetron sputtering. Appl Surf Sci 2009;255:4033–8.
[9] Sanchéz JE, Sanchéz OM, Ipaz L, Aperador W, Caicedo JC, Amaya C, et al. Mechanical, tribological, and electrochemical behavior of Cr_{1-x} Al_xN coatings deposited by r.f. reactive magnetron co-sputtering method. Appl Surf Sci 2010;256:2380–7.
[10] Wang YX, Zhang S, Lee J-W, Lew WS, Li B. Influence of bias voltage on the hardness and toughness of CrAlN coatings via magnetron sputtering. Surf Coat Technol 2012;206:5103–7.
[11] Lee JH, Ahn SH, Kim JG. Effect of Al additions in WC–$(Cr_{1-x}Al_x)$N coatings on the corrosion resistance of coated AISI D2 steel in a deaerated 3.5 wt.% NaCl solution. Surf Coat Technol 2005;190:417–27.
[12] Lin J, Mishra B, Moore JJ, Sproul WD. Microstructure, mechanical and tribological properties of $Cr_{1-x}Al_xN$ films deposited by pulsed-closed field unbalanced magnetron sputtering (P-CFUBMS). Surf Coat Technol 2006;201:4329–34.
[13] Lv Y, Ji L, Liu X, Li H, Zhou H, Chen J. Influence of substrate bias voltage on structure and properties of the CrAlN films deposited by unbalanced magnetron sputtering. Appl Surf Sci 2012;258:3864–70.
[14] Zheng K, Liu P, Li W, Ma F, Liu X, Chen X. Investigation on microstructure and properties of CrAlN/AlON nanomultilayers. Appl Surf Sci 2011;257:9583–6.
[15] Kim YJ, Byun TJ, Han JG. Bilayer period dependence of CrN/CrAlNnanoscale multilayer thin films. Superlattices Microstruct 2009;45:73–9.
[16] Nose M, Kawabata T, Watanuki T, Ueda S, Fujii K, Matsuda K, et al. Mechanical properties and oxidation resistance of CrAlN/BN nanocomposite coatings prepared by reactive dc and rf co-sputtering. Surf Coat Technol 2011;205:33–7.
[17] Li P, Chen L, Wang SQ, Yang B, Du Y, Li J, et al. Microstructure, mechanical and thermal properties of TiAlN/CrAlN multilayer coatings. Int J Refract Met Hard Mater 2013;40:51–7.
[18] Li W, Liu P, Zhao Y, Ma F, Liu X, Chen X, et al. Structure, mechanical properties and thermal stability of CrAlN/ZrO_2 nanomultilayers deposited by magnetron sputtering. J Alloys Compd 2013;562:5–10.
[19] Tlili B, Nouveau C, Walock MJ, Nasri M, Ghrib T. Effect of layer thickness on thermal properties of multilayer thin films produced by PVD. Vacuum 2012;86:1048–56.
[20] Tlili B. Caractérisation de films durs multicouches élaborés par pulvérisation magnétron. Influence des conditions d'élaboration sur leurs propriétés. Cluny-France: Arts et Métiers ParisTech; 2011 (PhD thesis).
[21] Uchida M, Nihira N, Mitsuo A, Toyoda K, Kubota K, Aizawa T. Friction and wear properties of CrAlN and CrVN films deposited by cathodic arc ion plating method. Surf Coat Technol 2004;177–178:627–30.
[22] Mahdavian SM, Mai YW, Cottrell B. Friction, metallic transfer and debris analysis of sliding surfaces. Wear 1982;82:221–32.
[23] Chim YC, Ding XZ, Zeng XT, Zhang S. Oxidation resistance of TiN, CrN, TiAlN and CrAlN coatings deposited by lateral rotating cathode arc. Thin Solid Films 2009;517:4845–9.
[24] Li CX, Xia J, Dong H. Sliding wear of TiAl intermetallics against steel and ceramics of Al_2O_3, Si_3N_4 and WC/Co. Wear 2006;261 (693–01).
[25] Cheng YH, Browne T, Heckerman B. Mechanical and tribological properties of CrN coatings deposited by large area filtered cathodic arc. Wear 2011;271:775–82.
[26] Lorenzo-Martin C, Ajayi O, Erdemir A, Fenske GR, Wie R. Effect of microstructure and thickness on the friction and wear behavior of CrN coatings. Wear 2013;302:963–71.
[27] Fontalvo GA, Daniel R, Mitterer C. Interlayer thickness influence on the tribological response of bi-layer coatings. Tribol Int 2010;43:108–12.

[28] Wiecinski P, Smolik J, Garbacz H, Kurzydlowski KJ. Microstructure and mechanical properties of nanostructure multilayer CrN/Cr coatings on titanium alloy. Thin Solid Films 2011;519:4069–73.
[29] Wang L, Nie X. Effect of annealing temperature on tribological properties and material transfer phenomena of CrN and CrAlN coatings. J Mater Eng Perform 2014;23(2):560–71.
[30] Kim YJ, Byun TJ, Han JG. Bilayer period dependence of CrN/CrAlN nanoscale multilayer thin films. Superlattices Microstruct 2009;45:73–9.
[31] Wang HW, Stack MM, Lyon SB, Hovsepian P, Münz WD. The corrosion behaviour of macroparticle defects in arc bond-sputtered CrN/NbN superlattice coatings. Surf Coat Technol 2000;126:279–87.
[32] Liu C, Bi Q, Leyland A, Matthews A. An electrochemical impedance spectroscopy study of the corrosion behaviour of PVD coated steels in 0.5 N NaCl aqueous solution: Part I. Establishment of equivalent circuits for EIS data modeling. Corros Sci 2003;45:1243–56.
[33] Liu C, Bi Q, Matthews A. EIS comparison on corrosion performance of PVD TiN and CrN coated mild steel in 0.5 N NaCl aqueous solution. Corros Sci 2001;43:1953–61.
[34] Subramanian B, Ananthakumar R, Jayachandran M. Structural and tribological properties of DC reactive magnetron sputtered titanium/titanium nitride (Ti/TiN) multilayered coatings. Surf Coat Technol 2011;205:3485–92.
[35] Chipatecua YL, Olaya JJ, Arias DF. Corrosion behaviour of CrN/Cr multilayers on stainless steel deposited by unbalanced magnetron sputtering. Vacuum 2012;86 (1393-01).
[36] Ahn SH, Lee JH, Kim JG, Han JG. Localized corrosion mechanisms of the multilayered coatings related to growth defects. Surf Coat Technol 2004;177–178:638–44.
[37] Song GH, Yang XP, Xiong GL, Zhou L, Chen LJ. The corrosive behavior of Cr/CrN multilayer coatings with different modulation periods. Vacuum 2013;89:136–41.
[38] Marulanda DM, Olaya JJ, Piratoba U, Mariño A, Camps E. The effect of bilayer period and degree of unbalancing on magnetron sputtered Cr/CrN nano-multilayer wear and corrosion. Thin Solid Films 2011;519:1886–93.
[39] Feng HP, Hsu CH, Lu JK, Shy YH. Effects of PVD sputtered coatings on the corrosion resistance of AISI 304 stainless steel. Mater Sci Eng, A 2003;347:123–9.
[40] Liu C, Leyland A, Lyon S, Matthews A. Electrochemical impedance spectroscopy of PVD-TiN coatings on mild steel and AISI316 substrates. Surf Coat Technol 1995;76-77:615–22.
[41] Ruden A, Restrepo-Parra E, Paladines AU, Sequeda F. Corrosion resistance of CrN thin films produced by dc magnetron sputtering. Appl Surf Sci 2013;270:150–6.
[42] Lewis DB, Creasey SJ, Wustefeld C, Ehiasarian AP, Hovsepian PE. The role of the growth defects on the corrosion resistance of CrN/NbN superlattice coatings deposited at low temperatures. Thin Solid Films 2006;503:143–8.